JOURNAL OF
REINFORCED
PLASTICS &
COMPOSITES

Article

Journal of Reinforced Plastics and Composites
31(21) 1467–1487

DOI: 10.1177/0731684412456330
jrp.sagepub.com
SAGE

Micromechanics-based progressive failure analysis of composite laminates using different constituent failure theories

Albert M Moncada[1], Aditi Chattopadhyay[1], Brett A Bednarcyk[2] and Steven M Arnold[2]

Abstract

Predicting failure in a composite can be performed using ply level mechanisms and/or micro level mechanisms. This paper uses the generalized method of cells and high-fidelity generalized method of cells micromechanics theories, coupled with classical lamination theory, to study progressive damage in composites. Different failure theories, implemented at the fiber and matrix constituent level within a laminate, are investigated. A comparison is made among maximum stress, maximum strain, Tsai-Hill, and Tsai-Wu failure theories. To verify the failure theories, the Worldwide Failure Exercise experiments are used. The Worldwide Failure Exercise is a comprehensive study that covers a wide range of polymer matrix composite laminates. The objectives of this paper are to evaluate the current predictive capabilities of the generalized method of cells and high-fidelity generalized method of cells micromechanics theories for the progressive failure prediction of polymer matrix composite laminates and to evaluate the influence of four failure criteria applied at the fiber/matrix constituent scale. The numerical results demonstrate overall agreement with the experimental results for most of the composite layups examined, but also point to the need for more accurate resin damage progression models.

Keywords

Micromechanics, composite material, failure, Worldwide Failure Exercise

Introduction

The goal of micromechanics is to predict the mechanical behavior of the composite material, given the arrangement and mechanical behavior of the constituent materials within a composite. If only effective elastic properties are required, the micromechanics problem simplifies considerably, and a number of micromechanics theories can provide reasonable results (see Herakovich[1] for examples and comparisons). If, however, local nonlinear effects, such as damage, debonding, and inelasticity need to be captured, the micromechanics theory must be capable of predicting the local stress and strain field gradients throughout the composite. Consequently, if the matrix at a particular location within the simulated composite reaches its yield or failure stress, a local deformation and/or damage model is utilized to predict the inelastic strain accumulation and/or damage response.[2–12] A key advantage of micromechanics vs. macromechanics of a ply is the ability to apply such nonlinear models at the constituent scale, where simpler monolithic damage and inelasticity models can be used.

In this paper, the generalized method of cells (GMC) and high-fidelity generalized method of cells (HFGMC) micromechanics theories, coupled with classical lamination theory[1,13] (as implemented within NASA's Micromechanics Analysis Code with Generalized Method of Cell (MAC/GMC)[14]), are employed to

[1]Department of Mechanical and Aerospace Engineering, School of Engineering of Matter, Transport and Energy, Arizona State University, Tempe, AZ, USA
[2]NASA Glenn Research Center, Cleveland, OH, USA

Corresponding author:
Albert M Moncada, Department of Mechanical and Aerospace Engineering, School of Engineering of Matter, Transport and Energy, Arizona State University, Tempe, AZ, USA.
Email: amoncada@asu.edu

predict the Worldwide Failure Exercise (WWFE) laminate behavior. The WWFE is a collection of comprehensive experiments that covers a wide range of polymer matrix composites (PMCs).[15,16] Six laminates were used to achieve a broad range of layups. They included different types of constituent materials (fiber and matrix), layups of the laminates (unidirectional, angle-ply, cross-ply, quasi-isotropic), and loading conditions. The contributors to the exercise were given the same material data for the plies and constituents. The WWFE data was then compared with the different PMC failure theory predictions from various authors.[17,18] It should be noted that the WWFE was geared towards ply level failure analysis methods rather than micromechanics based methods like those employed herein. Thus, while basic fiber and matrix elastic and strength properties were provided, additional data needed to accurately capture the nonlinear neat resin response curves were not.

Most of the contributors to the WWFE used lamina level mechanics for their theories. There were some that used some micromechanics properties in the formulation for other uses such as failure strain limits, post-failure analysis, failure criterion, and stress magnification factors. Chamis[17] was the only contributor in the original exercise that used full micromechanics theories for finding the laminate responses. When the WWFE continued in 2002,[19] two new micromechanics-based theories were added by Mayes and Hansen[20] using a multi-continuum theory and by Huang[21] using a bridging theory. All of these contributors started off with the constituent properties but used varying factors to match them to ply level properties, whereas this work does not.

The focus of the current study is to examine the influence of the choice of failure criterion (i.e., maximum stress, maximum strain, Tsai-Hill, and Tsai-Wu) for a given constituent (microscale) on the overall ability to predict composite failure at the macroscale. Note that no modifications are made to account for the in-situ behavior of the constituents. Rather, pure predictions are made using the constituent properties provided by the WWFE. As such, the predictions presented here do not benefit from the ''anchor points'' along the axes in a ply level failure envelope plot that correspond to ply tensile and compressive strengths. The anchor points in the present model are *predicted* from the constituent level elastic and strength properties. Consequently, it is expected that the overall correlation of the numerical simulations with experiment could benefit from backing out in-situ properties, which would enable significantly better matching of the ply level response. This study was performed to show the feasibility of this method to use constituent properties and generate lamina and laminate responses that perform comparably to properties generated from ply level testing. Furthermore, a basic step function (i.e., subvolume elimination) has been employed to simulate damage progression at the fiber/matrix scale. Namely, once a subvolume within the micromechanics model satisfies the applicable failure criterion, it is then instantaneously assigned a near zero stiffness. Again, the predictions should benefit from a more progressive transition from damage initiation to complete loss of stiffness on the micro scale, but this was not attempted in this study. The results presented herein should thus be interpreted as a preliminary application of GMC and HFGMC to PMC laminate failure with an eye toward identifying areas for improvement and the influence of failure criterion selection on the overall composite response and failure.

Background

The family of micromechanics theories, known collectively as the GMC, has been employed in the present paper. These methods provide semi-closed form expressions for the effective constitutive behavior of a composite material, including nonlinear effects such as damage, debonding, and inelasticity, which can be modeled internally based on the local fiber and matrix stress and strain fields. The original method of cells[22,23] considered a doubly periodic repeating unit cell (applicable for continuous reinforcement) and was limited to only four subcells (one fiber and three matrix). This theory was generalized by Paley and Aboudi[24] to consider an arbitrary number of subcells and thus constituent phases. The resulting GMC thus enables analysis of repeating unit cells containing more than two constituent materials, a more refined fiber shape, and various fiber architectures (i.e., fiber packing arrangements). A triply periodic version of GMC has also been developed,[25] which models short fiber and particulate reinforced composites, as well as porous materials.

Fundamental to GMC is the assumed linear displacement field, which produces subcells with a state of constant stress and strain. Therefore, no additional quadrature points are necessary within each subcell to track nonlinear effects; a single subcell value (at the centroid) for each component will suffice. Also, these constant stress and strain fields result in a lack of normal to shear coupling which limits the accuracy of GMC's local stress and strain fields. That is, if only global normal loads are applied, then locally, only normal stresses are produced. Similarly, if only global shear loads are applied, then only local shear stresses are generated. On the positive side, GMC's lack of shear coupling enables the method's equations to be reformulated such that unique tractions serve as the basic unknowns, which significantly increase the computational efficiency of the method by hundreds to

thousands of times for sufficiently complex repeating unit cells.[26,27] Finally, due to the constant fields, GMC is completely insensitive to subcell grid refinement, as long as the architecture of the repeating unit cell is not altered by such grid refinement. Consequently, the least refined representation of a given Representative Unit Cell (RUC) architecture that allows for the capturing of the salient features of the microstructural geometry will suffice.

A newer but related micromechanics model, HFGMC, has overcome GMC's lack of normal and shear coupling[28,29] by assuming a second order Taylor series expansion for each subcell's displacement field, along with additional equations required to enforce continuity and periodicity. The result is more accurate at local stress and strain fields, but at the expense of more intensive computational demands. Further, HFGMC exhibits subcell grid refinement dependence (although less extreme than typical finite element mesh refinement), along with the need to track field variables at quadrature points within each subcell to account for nonlinear inelastic effects. Aboudi[30,31] has provided review papers summarizing the work done to date by researchers around the world using both the GMC and HFGMC micromechanics theories.

Failure theories

The failure theories compared herein, all of which are applied on the fiber/matrix constituent level, are the maximum stress, maximum strain, Tsai-Hill, and Tsai-Wu criteria. A comparison of these failure theories applied at the ply level is provided by Herakovich.[1] The maximum stress criterion can be expressed as

$$\begin{array}{ll} X_C < \sigma_{11} < X_T & |\tau_{23}| < Q \\ Y_C < \sigma_{22} < Y_T & |\tau_{13}| < R \\ Z_C < \sigma_{33} < Z_T & |\tau_{12}| < S \end{array} \tag{1}$$

where the stress components are subcell values, X_T, Y_T, and Z_T are the tensile material normal strengths, X_C, Y_C, and Z_C are the compressive material normal strengths, and Q, R, and S are the material shear strengths. Note that compressive strengths are negative. Violation of any part of equation (1) indicates failure of the subcell.

Similarly, the maximum strain criterion can be written as,

$$\begin{array}{ll} X_{\varepsilon C} < \varepsilon_{11} < X_{\varepsilon T} & |\gamma_{23}| < Q_\varepsilon \\ Y_{\varepsilon C} < \varepsilon_{22} < Y_{\varepsilon T} & |\gamma_{13}| < R_\varepsilon \\ Z_{\varepsilon C} < \sigma_{33} < Z_{\varepsilon T} & |\gamma_{12}| < S_\varepsilon \end{array} \tag{2}$$

where the strain components are subcell values, $X_{\varepsilon T}$, $Y_{\varepsilon T}$, and $Z_{\varepsilon T}$ are the tensile material normal failure strains, $X_{\varepsilon C}$, $Y_{\varepsilon C}$, and $Z_{\varepsilon C}$ are the compressive material normal failure strains, and Q_ε, R_ε, and S_ε are the material shear failure. Note that compressive failure strains are negative. Violation of any part of equation (2) indicates failure of the subcell.

The fully multiaxial Tsai-Hill criterion[32] failure surface is expressed as,

$$\begin{aligned} &\frac{\sigma_{11}^2}{X^2} + \frac{\sigma_{22}^2}{Y^2} + \frac{\sigma_{33}^2}{Z^2} + \frac{\tau_{23}^2}{Q^2} + \frac{\tau_{13}^2}{R^2} + \frac{\tau_{12}^2}{S^2} \\ &\quad - \sigma_{11}\sigma_{22}\left(\frac{1}{X^2} + \frac{1}{Y^2} - \frac{1}{Z^2}\right) \\ &\quad - \sigma_{11}\sigma_{33}\left(\frac{1}{X^2} - \frac{1}{Y^2} + \frac{1}{Z^2}\right) \\ &\quad - \sigma_{22}\sigma_{33}\left(-\frac{1}{X^2} + \frac{1}{Y^2} + \frac{1}{Z^2}\right) = 1 \end{aligned} \tag{3}$$

where, in order to incorporate differing tensile and compressive strengths, X, Y, and Z have the additional constraints:

$$X = \begin{cases} X_T & \sigma_{11} \geq 0 \\ X_C & \sigma_{11} < 0 \end{cases} \quad Y = \begin{cases} Y_T & \sigma_{22} \geq 0 \\ Y_C & \sigma_{22} < 0 \end{cases} \quad Z = \begin{cases} Z_T & \sigma_{33} \geq 0 \\ Z_C & \sigma_{33} < 0 \end{cases} \tag{4}$$

Subcell failure is indicated when the function on the left-hand side of equation (3) is greater than 1. Finally, the Tsai-Wu failure surface[33] can be written as,

$$\begin{aligned} &\sigma_{11}\left(\frac{1}{X_T} + \frac{1}{X_C}\right) + \sigma_{22}\left(\frac{1}{Y_T} + \frac{1}{Y_C}\right) + \sigma_{33}\left(\frac{1}{Z_T} + \frac{1}{Z_C}\right) \\ &\quad - \frac{\sigma_{11}^2}{X_T X_C} - \frac{\sigma_{22}^2}{Y_T Y_C} - \frac{\sigma_{33}^2}{Z_T Z_C} + \frac{\tau_{23}^2}{Q^2} + \frac{\tau_{13}^2}{R^2} + \frac{\tau_{12}^2}{S^2} \\ &\quad + 2F_{12}\sigma_{11}\sigma_{22} + 2F_{13}\sigma_{11}\sigma_{33} + 2F_{23}\sigma_{22}\sigma_{33} = 1 \end{aligned} \tag{5}$$

where the compressive strengths are negative. The interaction coefficients, F_{12}, F_{13}, and F_{23}, herein have been taken according to Tsai and Hahn,[34]

$$F_{12} = -\frac{1}{2\sqrt{X_T X_C Y_T Y_C}} \quad F_{13} = -\frac{1}{2\sqrt{X_T X_C Z_T Z_C}} \quad F_{23} = -\frac{1}{2\sqrt{Y_T Y_C Z_T Z_C}} \tag{6}$$

Note that the Tsai-Wu theory with the interaction terms taken according to Reference 20 have been denoted "Tsai-Wu (Hahn)". Subcell failure is indicated when the function on the left-hand side of equation (6) is greater than 1.

The use of these failure criteria has both advantages and disadvantages.[35] For the maximum stress and maximum strain theories, the implementation is very

simple. The drawback of these two failure criteria is that they do not account for any interactions among the stress components. The advantage of using the Tsai-Hill and Tsai-Wu (Hahn) failure criteria is that they account for interaction among the stress components. The disadvantages are that they are more complex, and the Tsai-Wu criterion introduces additional coefficients. If the material is isotropic, the Tsai-Hill failure criteria reduces to the von Mises failure criterion. The Tsai-Wu (Hahn) failure criteria was incorporated into these simulations so the effects of hydrostatic stress could be included since they are omitted in the Tsai-Hill criteria. Both the Tsai-Hill and Tsai-Wu criterion have been implemented into GMC in order to model failure of both isotropic and orthotropic constituent materials.

Numerical analysis and results

The considered materials, laminate lay-ups, and loading cases are shown in Table 1 and were extracted from References 2. Schematics of these laminates used are shown in Figure 1, with the fiber orientation and

Table 1. Summary of composite laminates and specific loading cases examined for each composite system.[16]

Material	Laminate lay-up	Loading case and description
AS4/3501-6	$(0^\circ/\pm 45^\circ/90^\circ)_s$ laminate	1. σ_y vs σ_x failure stress envelope
		2. Stress/strain curve for σ_y:$\sigma_x = 1{:}0$
		3. Stress/strain curve for σ_y:$\sigma_x = 2{:}1$
T300/BSL914C	0° unidirectional lamina	4. σ_x vs τ_{xy} failure stress envelope
E-glass/LY556/HT907/DY063	0° unidirectional lamina	5. σ_y vs τ_{xy} failure stress envelope
	$(90^\circ/\pm 30^\circ)_s$ laminate	6. σ_y vs σ_x failure stress envelope
		7. σ_x vs τ_{xy} failure stress envelope
E-glass/MY750/HY917/DY063	0° unidirectional lamina	8. σ_y vs σ_x failure stress envelope
	$(0^\circ/90^\circ)_s$ cross ply laminate	9. Stress/strain curve for σ_y:$\sigma_x = 0{:}1$
	$(\pm 55^\circ)_s$ angle ply laminate	10. σ_y vs σ_x failure stress envelope
		11. Stress/strain curve for σ_y:$\sigma_x = 1{:}0$
		12. Stress/strain curve for σ_y:$\sigma_x = 2{:}1$
	$(\pm 45^\circ)_s$ angle ply laminate	13. Stress/strain curve for σ_y:$\sigma_x = 1{:}1$
		14. Stress/strain curve for σ_y:$\sigma_x = 1{:}-1$

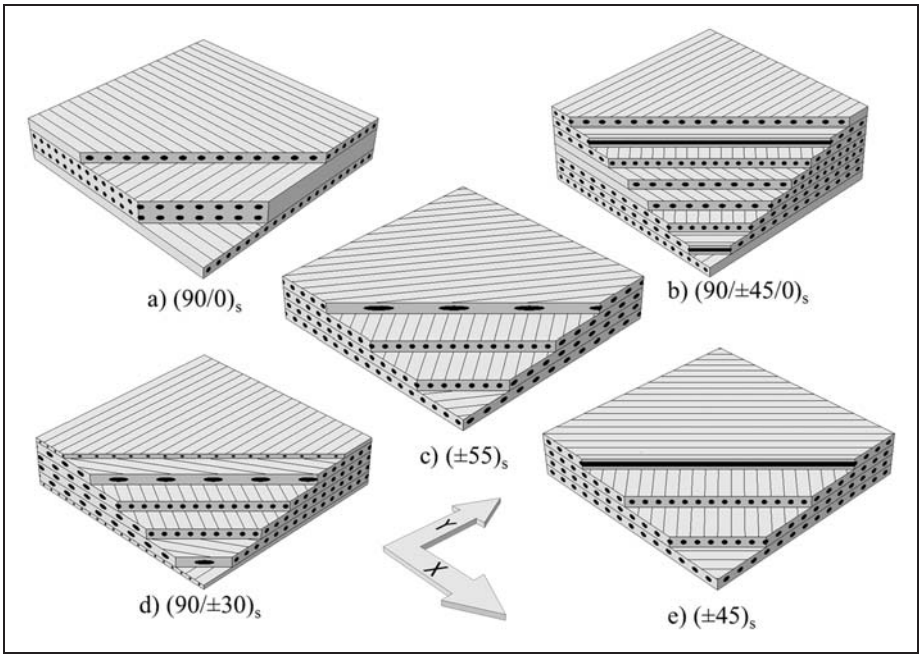

Figure 1. Laminate composite layup orientations for a) $(90/0)_s$, b) $(90/\pm 45/0)_s$, c) $(\pm 55)_s$, d) $(90/\pm 30)_s$, and e) $(\pm 45)_s$.

relative layer thickness shown to scale. The constituent material properties are shown in Tables 2 and 3.

The results presented below are pure predictions based on the fiber/matrix constituent properties provided in Reference 2. A linear elastic constituent model is used until the material has reached the failure criteria. Within this constituent model, the simplest damage progression model, a step function, has been employed herein. That is, once a subcell has reached failure according to the applicable failure criterion, its stiffness is instantaneously reduced to 0.01% of its original value. This is done identically regardless of the mode of failure. In the case of HFGMC, where stresses vary within a subcell, the subcell average stress is employed to predict failure. Clearly, a much more involved failure progression model can be incorporated in the future, and within HFGMC, subcell quadrature point-based failure, rather than subcell average failure, could be considered. In all cases, the 26×26 subcell repeating unit cell, shown in Figure 2, was employed. Note that this repeating unit cell is quite refined in

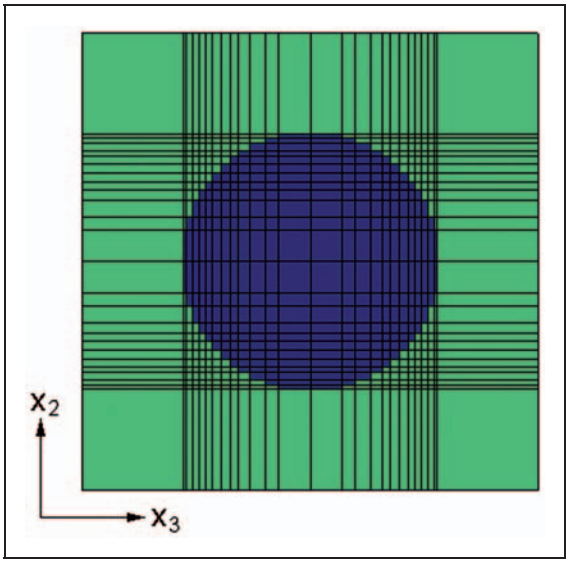

Figure 2. GMC and HFGMC 2626 subcell repeating unit cell employed to model the plies in the various WWFE laminates.

Table 2. Fiber material properties.[16]

Fiber type	AS4	T300	E-glass Gevetex	E-glass Silenka
Longitudinal modulus, E_{f1} (GPa)	225	230	80	74
Transverse modulus, E_{f2} (GPa)	15	15	80	74
In-plane shear modulus, G_{f12} (GPa)	15	15	33.33	30.8
Major Poisson's ratio, ν_{12}	0.2	0.2	0.2	0.2
Transverse shear modulus, G_{f23} (GPa)	7	7	33.33	30.8
Longitudinal tensile strength, X_{fT} (MPa)	3350	2500	2150	2150
Longitudinal compressive strength, X_{fc} (MPa)	2500	2000	1450	1450
Longitudinal tensile failure strain, f_{1T} (%)	1.488	1.086	2.687	2.905
Longitudinal compressive failure strain, f_{1C} (%)	1.111	0.869	1.813	1.959

Table 3. Matrix material properties.[16]

Matrix type	3501-6 epoxy	BSL914C epoxy	LY556/HT907/ DY063 epoxy	MY750/HY917/ DY063 epoxy
Manufacturer	Hercules	DFVLR	Ciba Geigy	Ciba Geigy
Modulus, E_m (Gpa)	4.2	4	3.35	3.35
Shear modulus, G_m (GPa)	1.567	1.481	1.24	1.24
Poisson's ratio, ν_{12}	0.34	0.35	0.35	0.35
Tensile strength, Y_{mT} (MPa)	69	75	80	80
Compressive strength, Y_{mC} (MPa)	250	150	120	120
Shear strength, S_m (MPa)	50	70	–	–
Tensile failure strain, ε_{mT} (%)	1.7	4	5	5

terms of those typically used in GMC and HFGMC[26,29] and is sufficient for capturing the local fields accurately in the context of these models.

For the failure surfaces within this work, both the initial and final failures are shown. The experimental values are shown as open circles while the four different subcell failure criteria are represented as various line types. In each case, the predicted initial failure envelope is of the same type as its associated final failure line type, except for the addition of symbols to the line type. There are, however, some cases where the initial failure is not shown because it is only 1 to 2 MPa from the final failure surface. These cases were all of the unidirectional laminas (Figures 3, 4, and 5) and the failure surface for the $\pm(55)_s$ laminate, Figure 6.

The percent error equation used for quantifying the error in the plots is shown in equation (7). Two

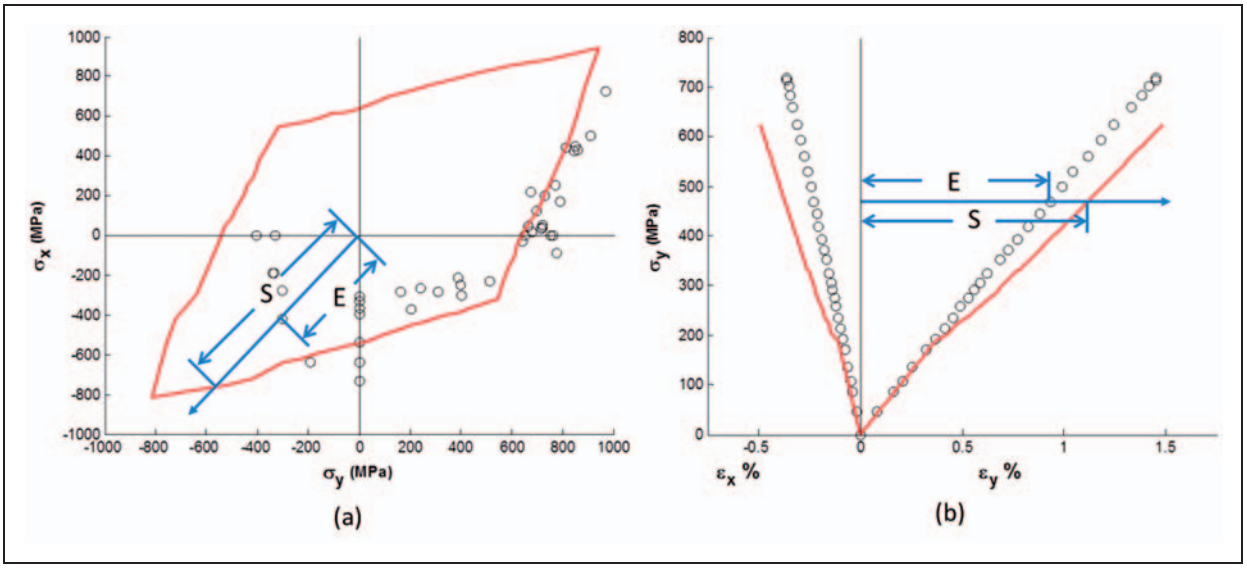

Figure 3. Method for calculating E and S for percent error calculation for (a) failure surfaces and (b) stress-strain curves.

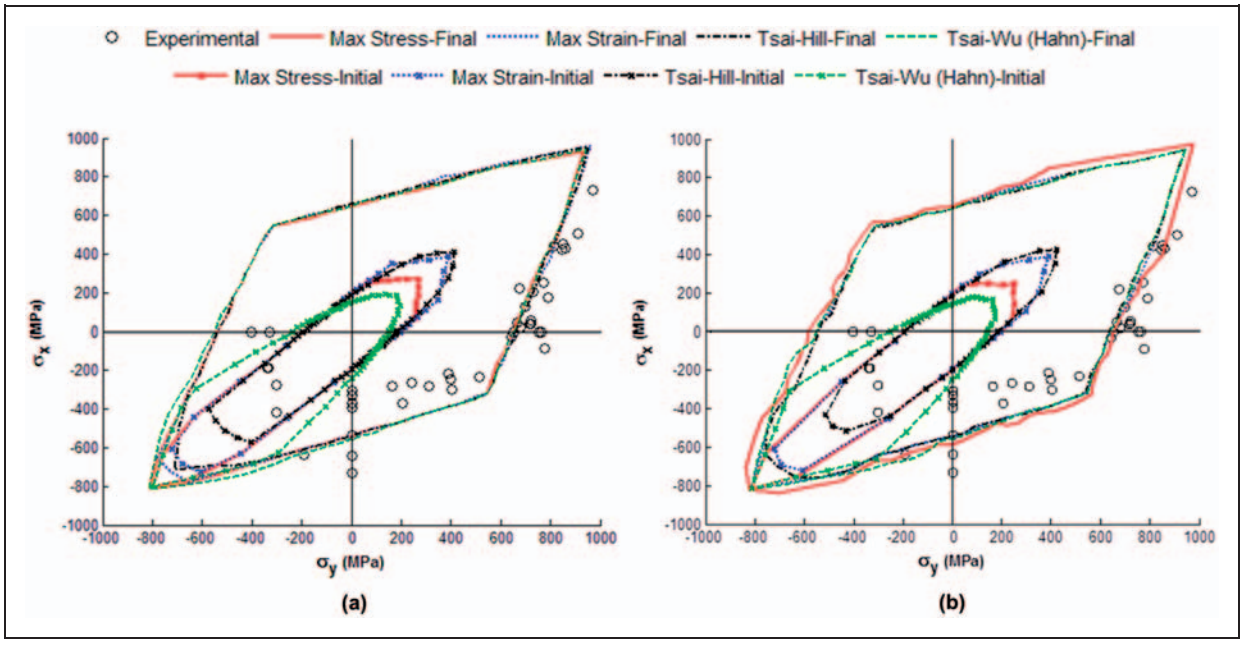

Figure 4. (0°/±45°/90°) laminate AS4/3501-6: σ_y vs σ_x failure stress envelope with (a) GMC and (b) HFGMC.

methods were used to calculate the distances between the simulation (S) and experiment (E) within the failure surfaces and stress–strain curves. Figure 7 shows how E and S are calculated for the failure surface. The magnitude for the experiment is measured from the origin to the experimental point, E. The same loading ratio is used and the value on the simulated failure surface is acquired as S. This is then averaged for all the experimental points. If there are common experimental points along a similar loading ratio, the mean is calculated and used as E for that loading ratio. For calculating the magnitudes for the stress–strain curves, a horizontal line is drawn from the vertical axis through the experimental point and through the simulation. The percent

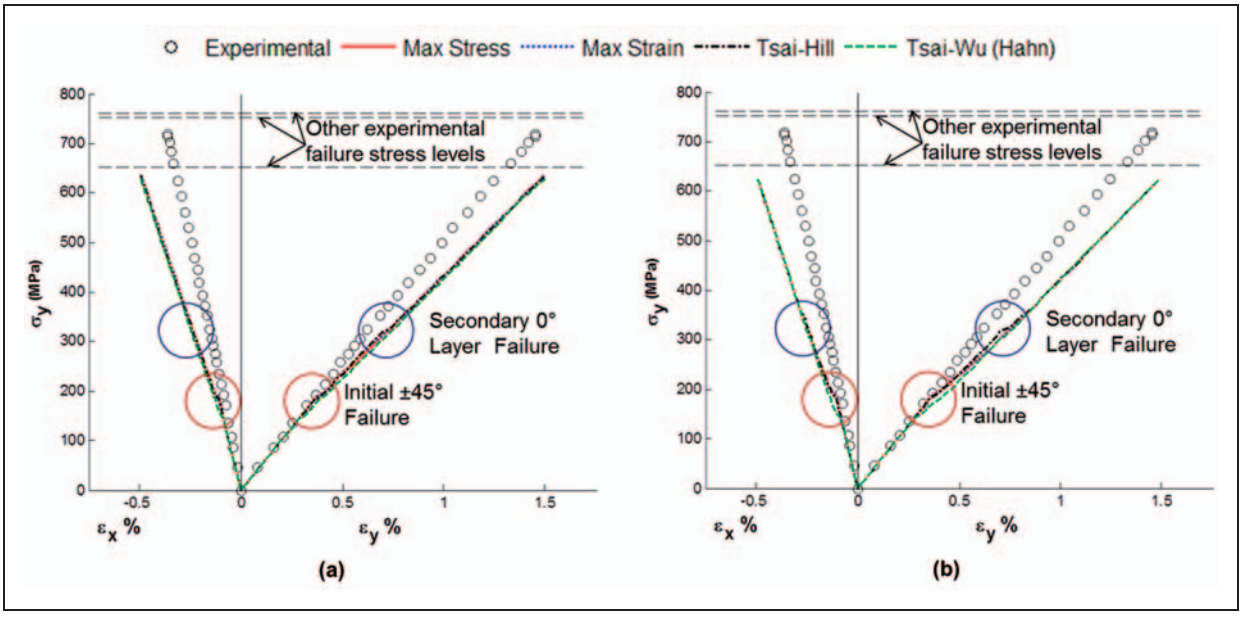

Figure 5. (0°/±45°/90°) laminate AS4/3501-6: Stress/strain curves for $\sigma_y : \sigma_x = 1 : 0$ with (a) GMC and (b) HFGMC.

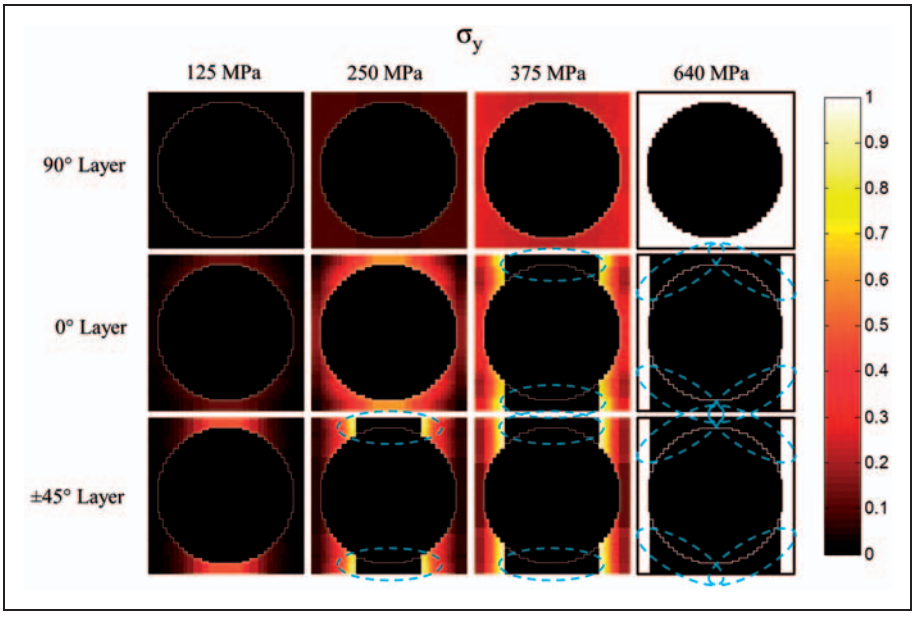

Figure 6. Tsai-Hill plots of Representative Unit Cell for (0°/±45°/90°) laminate with loading of $\sigma_y : \sigma_x = 1 : 0$ using GMC. The failed subcells are circled with blue ellipses. RUC: Representative Unit Cell.

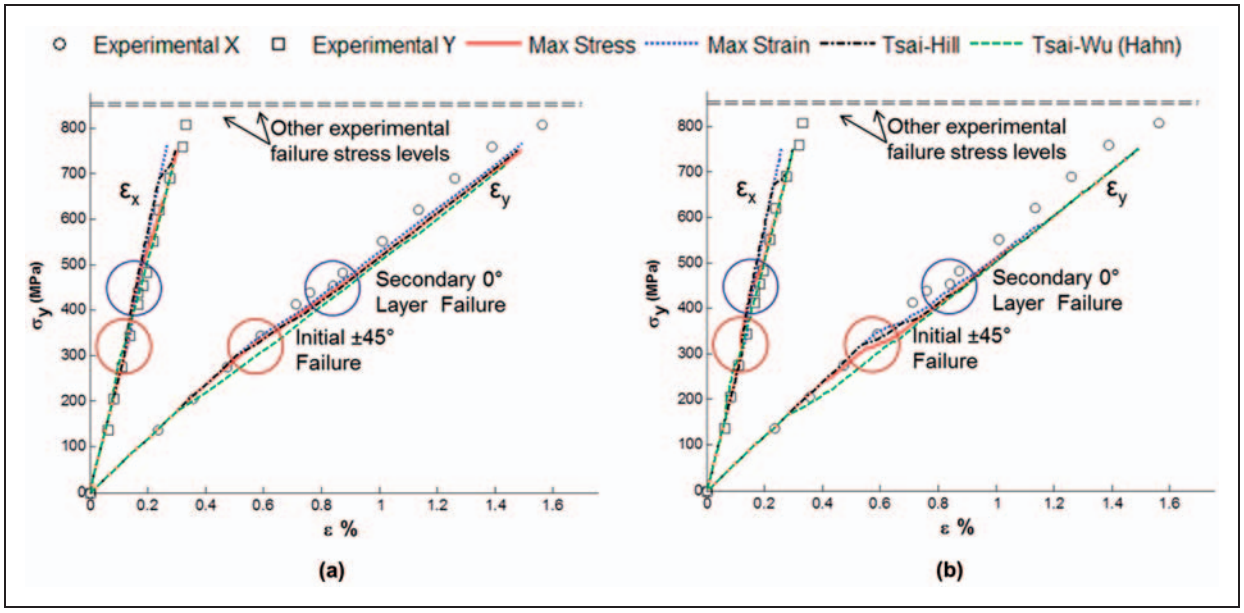

Figure 7. (0°/±45°/90°) laminate AS4/3501-6: Stress/strain curve for $\sigma_y:\sigma_x = 2:1$ with (a) GMC and (b) HFGMC.

error is again calculated for all the experimental points and averaged.

$$\%\ \text{error} = \frac{|S-E|}{E} \times 100 \tag{7}$$

(0°/±45°/90°) laminate, AS4/3501-6: σ_y vs σ_x failure stress envelope. A comparison of theoretical predictions to experimental results for the failure stress envelope in the global directions (*X*, *Y*), see Figure 1, is shown in Figure 4(a) for GMC and Figure 4(b) for HFGMC. The GMC and HFGMC simulations predict final failure that is similar for all failure theories, with HFGMC predicting somewhat wider failure initiation envelopes. This could be attributed to the quasi-isotropic laminate washing out the intricacies of each failure theory. This is verified by calculating the percent error associated with the failure surfaces, Table 4. Also, from Table 4 we can see that the Tsai-Hill and Max Strain failure criteria were ranked first and second, respectively, for both GMC and HFGMC simulations. The final failure envelopes are similar for the failure criteria for the first, second, and fourth quadrants. The failure criteria show good agreement with experiment in the first and fourth quadrants, while the second quadrant has no experimental data. There is an over-prediction for all criteria in the third quadrant, which could be attributed to specimen buckling. The over-prediction in this quadrant contributes to most of the error for all of the failure surfaces. In the initial failure envelope, all the failure criteria are similar for the second and fourth quadrant, but vary in the first and third. It should be noted that there is clear variability among criteria for damage initiation, but all the failure criteria are very close for predicting final failure. It seems that final failure is controlled more by how damage progresses, which is not as dependent on the particular failure criterion.

Table 4. Percent error for AS4/3501-6 failure stress envelope for both GMC and HFGMC

	GMC		HFGMC	
	% Error	Rank	% Error	Rank
Max stress	32.1	3	36.6	4
Max strain	31.5	2	32.8	2
Tsai-Hill	30	1	32.5	1
Tsai-Wu (Hahn)	33.6	4	33.4	3

GMC: generalized method of cells; HFGMC: high-fidelity generalized method of cells.

(0°/±45°/90°) laminate, AS4/3501-6: stress/strain curves for $\sigma_y:\sigma_x = 1:0$. A comparison of theoretical predictions to experimental results for tension loading along the y-direction is shown in Figure 5(a) for GMC and Figure 5(b) for HFGMC. The experimental values are shown as open circles while the four different subcell failure criteria are shown with various line types as denoted in the legend.

All of the failure criteria predictions are similar to one another, as are the predictions of GMC and HFGMC. The onset of initiation of damage (as indicated by deviation from linearity) between the experiments and the predictions is very good as well. Subsequent to initiation, the simulations exhibit both a lower secondary slope and ultimate composite failure

stress than the experimental results. This is similar to the results from the ply level theory of Bogetti et al.[36] for this load case. Figure 6 illustrates the magnitude of the Tsai-Hill failure criterion at the microscale, thus enabling one to observe the onset of failure in the fiber and matrix using GMC. Failure occurs when the values surpass the critical value of 1 whereupon the corresponding subcell stiffness is reduced to approximately zero and thus reducing its load carry ability. Within the figure, the failed subcells are circled with blue ellipses. From Figure 6 it is clear that the initial ply failure starts in between 125 and 250 MPa within the matrix of the ±45° layers which corresponds to the main stiffness change shown in Figure 5. The second ply failure, within the 0° layer, occurs between 250 and 375 MPa, which corresponds to the minor shifts in Figure 5. The final failure of the 90° layer caused the complete laminate failure.

The percent errors for the four failure theories are shown in Table 5 for both GMC and HFGMC. As was shown in Figure 5, the percent errors for all of the failure theories are low with the best being the Max Stress and Max Strain for both GMC and HFGMC.

(0°/±45°/90°) laminate, AS4/3501-6: stress/strain curves for σ_y:σ_x = 2:1. A comparison of theoretical predictions to experimental results for combined tension loading ($\sigma_y = 2\ \sigma_x$) is shown in Figure 7(a) for GMC and Figure 7(b) for HFGMC. The experimental values are shown as open circles for the strain along the x-direction and open squares for the strain along the y-direction, while the four different subcell failure criteria are shown with various denoted line types.

The various failure criteria predictions are similar to one another. In the GMC case, the failure criteria under-predict the final failure and over predict the nonlinearity caused by progressive failure. The progression of subcell and ply failure can again be observed by plotting the Tsai Hill failure criteria (for example) as shown in Figure 8. Again within the figure, the failed subcells are circled with blue ellipses. The ply matrix

Table 5. (0°/±45°/90°) laminate AS4/3501-6 percent error for the stress/strain curves with σ_y:σ_x = 1:0 loading for both GMC and HFGMC

	GMC				HFGMC			
	ε_x % error	ε_y % error	Average % error	Rank	ε_x % error	ε_y % error	Average % error	Rank
Max stress	5.5	5.5	5.5	1	7.2	5.7	6.5	1.5
Max strain	5.0	7.4	6.2	2	5.4	7.6	6.5	1.5
Tsai-Hill	5.8	8.6	7.2	4	6.8	8.3	7.6	4
Tsai-Wu (Hahn)	8.7	4.7	6.7	3	9.6	3.7	6.7	3

GMC: generalized method of cells; HFGMC: high-fidelity generalized method of cells.

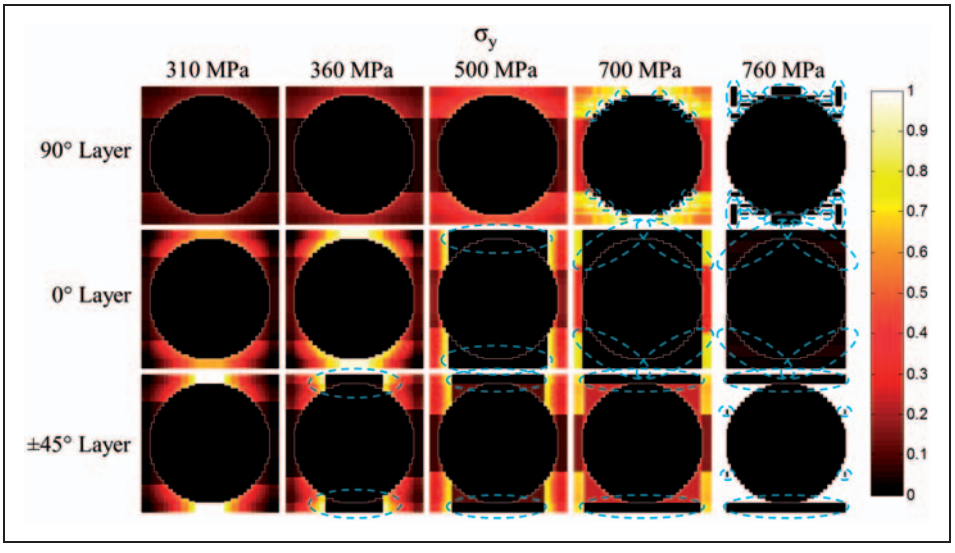

Figure 8. Tsai-Hill plots of Representative Unit Cell for (0°/±45°/90°) laminate with loading of $\sigma_y : \sigma_x = 2 : 1$ using GMC. The failed subcells are circled with blue ellipses. RUC: Representative Unit Cell.

subcell failures correspond to the changes in slope of composite stress–strain response with the initial, secondary, and final failure occurring within the ±45°, 0°, and 90° layers, respectively. The percent error for both GMC and HFGMC predictions are very similar for the Max Stress, Max Strain, and Tsai Hill (see Table 6), with the Tsai-Wu (Hahn) theory displaying slightly higher error.

0° lamina, T300/BSL914C: σ_x vs τ_{xy} failure stress envelope. A comparison of theoretical predictions and experimental results for the transverse and shear loading failure stress envelope is shown in Figure 9(a) for GMC and Figure 9(b) for HFGMC. The percent error is similar among all of the failure theories, Table 7. The difference between the predicted failure shear stress of all the failure criteria and the median failure of the experiments is 20 MPa for GMC and 19 MPa HFGMC. There is a large scatter between the high and low of the experimental data for the shear stress alone, with the high being 101.3 MPa and low being 55.2 MPa. This makes it difficult to give an accurate deviation between the experimental and predicted data for pure shear loading, although the models are clearly significantly under predicting the shear failure. The deviation between GMC and HFGMC, however, is small, therefore suggesting that the cause lies somewhere other than the micromechanics formulation. The large amount of scatter within the experimental results of Figure 9 indicate that capturing stochastic effects in the model would be advantageous. There is not much scatter between the various failure criteria, but this could be attributed to the large discrepancy between the shear and axial failure stresses. There is a slight variation when the failure mechanism switches between tension and the shear failures.

0° lamina, E-glass/LY556/HT907/DY063: σ_y vs τ_{xy} failure stress envelope. A comparison of theoretical predictions to experimental results for the transverse and

Table 6. (0°/±45°/90°) laminate AS4/3501-6 percent error for the stress/strain curves with σ_y:σ_x = 2:1 loading for both GMC and HFGMC

	GMC				HFGMC			
	ε_x % error	ε_y % error	Average % error	Rank	ε_x % error	ε_y % error	Average % error	Rank
Max stress	40.1	12.4	26.3	2	43.3	14.6	29.0	2.5
Max strain	40.5	11.9	26.2	1	43.3	14.6	29.0	2.5
Tsai-Hill	40.5	12.2	26.4	3	43.5	13.6	28.6	1
Tsai-Wu (Hahn)	41.7	14.8	28.3	4	43.5	16.7	30.1	4

GMC: generalized method of cells; HFGMC: high-fidelity generalized method of cells.

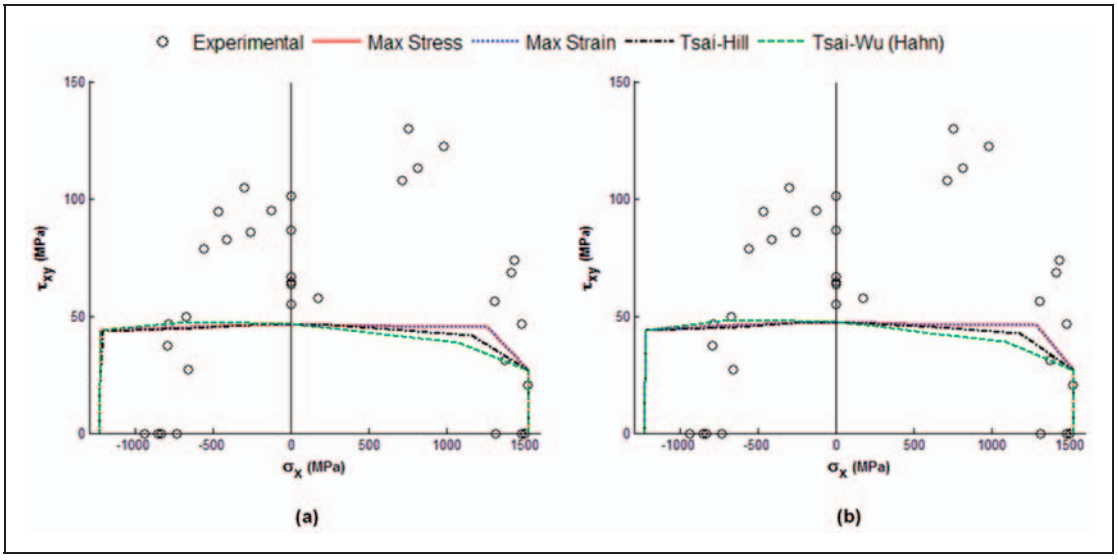

Figure 9. 0° lamina T300/BSL914C: σ_x vs τ_{xy} failure stress envelope with (a) GMC and (b) HFGMC.

shear loading failure stress envelope is shown in Figure 10(a) for GMC and Figure 10(b) for HFGMC. The best fit for the experimental data was the Tsai-Wu (Hahn) failure criteria, which offered good correlation with the transverse tension and compression loading. The percent error quantifies how well the Tsai-Wu (Hahn) performed compared to the other failure theories, see Table 8. The pure shear loading was under-predicted by approximately 18 MPa for all failure criteria, which was a percent error of 29.2%. The pure shear loading, however, improved to 13 MPa under-prediction using HFGMC which was a percent error of 21.6%. There also is an interaction with the shear stress and transverse compressive stress in the experiments that delays failure that the models did not capture. The correlation would clearly benefit from using in-situ constituent properties, which would allow the model to reproduce the pure shear loading data point. The differences between the GMC and HFGMC models are small compared to those among the various failure criteria. The Tsai-Hill envelope shows the greatest deviation between GMC and HFGMC. This case is very different than the first failure surface case in which the final failure surfaces are very similar. This could be attributed to this system being a single lamina. Within the other laminates, the various stacking sequences helped mask this effect.

$(90°/\pm 30°/90°)$ laminate, E-glass/LY556/HT907/DY063: σ_y vs σ_x failure stress envelope. A comparison of theoretical predictions to experimental results for the failure stress envelope in the normal directions is shown in Figure 11(a) for GMC and in Figure 11(b) for HFGMC. All the failure theories seem to be consistent with one another with minor deviations for both the GMC and HFGMC final failure envelopes, except for the Tsai-Wu (Hahn) wherein significant variation between GMC and HFGMC is observed. Both have varying initial failure envelopes with significant differences in the third quadrant (although little experimental

Table 7. Percent error for T300/BSL914C failure stress envelope for both GMC and HFGMC

	GMC		HFGMC	
	% Error	Rank	% Error	Rank
Max stress	37.6	1.5	37.1	1.5
Max strain	37.6	1.5	37.1	1.5
Tsai-Hill	38	3	37.4	3
Tsai-Wu (Hahn)	39.5	4	39.1	4

GMC: generalized method of cells; HFGMC: high-fidelity generalized method of cells.

Table 8. Percent error for E-glass/LY556/HT907/DY063 σ_y vs τ_{xy} failure stress envelope for both GMC and HFGMC

	GMC		HFGMC	
	% Error	Rank	% Error	Rank
Max stress	36.5	2	36	2
Max strain	36.8	3	36.1	3
Tsai-Hill	38.1	4	38	4
Tsai-Wu (Hahn)	28	1	31.9	1

GMC: generalized method of cells; HFGMC: high-fidelity generalized method of cells.

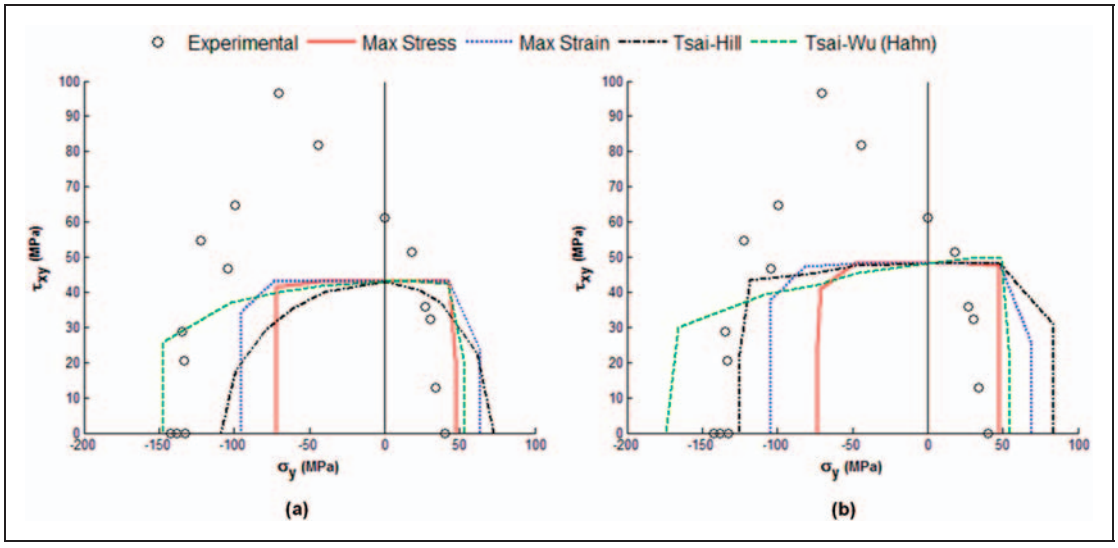

Figure 10. 0° lamina E-glass/LY556/HT907/DY063: σ_y vs τ_{xy} failure stress envelope with (a) GMC and (b) HFGMC.

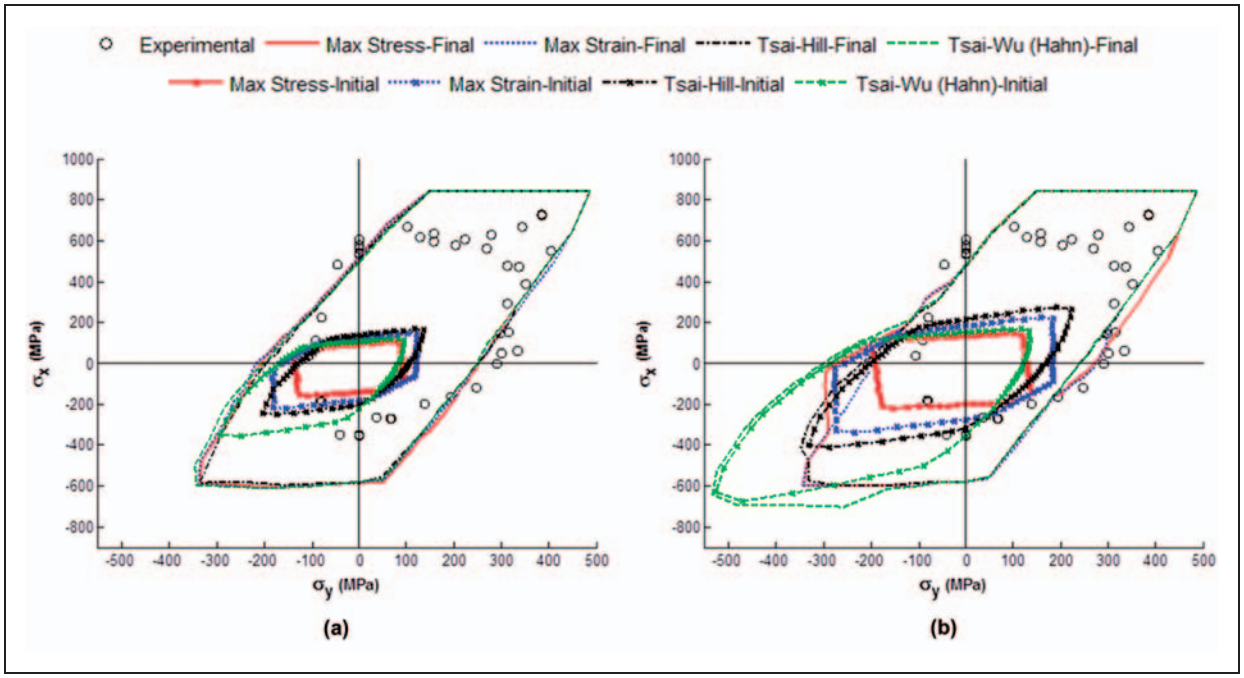

Figure 11. (90°/±30°/90°) laminate E-glass/LY556/HT907/DY063: σ_y vs σ_x failure stress envelope with (a) GMC and (b) HFGMC.

Table 9. Percent error for (90°/±30°/90°) laminate E-glass/LY556/HT907/DY063 σ_y vs σ_x failure stress envelope for both GMC and HFGMC

	GMC		HFGMC	
	% Error	Rank	% Error	Rank
Max stress	40.5	4	53.8	3
Max strain	40.4	3	44.2	2
Tsai-Hill	38.5	1	41.9	1
Tsai-Wu (Hahn)	40.2	2	60.7	4

GMC: generalized method of cells; HFGMC: high-fidelity generalized method of cells.

data is given in this quadrant). This is also where the failure prediction has the greatest deviation from the experimental data. This suggests the presence of a compressive failure mechanism (e.g., buckling, fiber kinking) that is not being captured by the models. There is a slight deviation in the second quadrant as well, but not as severe as in the third quadrant. The first and fourth quadrants agree well with the experimental data. Table 9 shows the errors to be high but this is skewed by the large discrepancies in the third quadrant. This laminate is behaving similar to the AS4/3501-6 laminate in the first test in which there is a clear variability among criteria for damage initiation, but all the failure criteria are very close for predicting final failure. This is true for all the cases except the Tsai-Wu (Hahn) using HFGMC.

(90°/±30°/90°) laminate, E-glass/LY556/HT907/DY063: σ_x vs τ_{xy} failure stress envelope. A comparison of theoretical predictions to experimental results for the failure stress envelope in the x-direction and shear loading is shown in Figure 12(a) for GMC and Figure 12(b) for HFGMC. The final failure envelopes are very similar to one another, except with the Max Strain failure criterion having a higher prediction for the pure shear stress failure for GMC. The failure criteria lead to an over-prediction for both pure shear and compression. The tension, on the other hand, is a slight under-prediction. The initial failure envelopes seem similar, but with slight variations. The initial failure envelopes for the HFGMC tend to occur at higher stresses than those in GMC. Overall, the predictions for this laminate have the general shape of the experimental failure envelope. Table 10 shows that the Tsai-Hill and Tsai-Wu (Hahn) had the lowest percentage error for both GMC and HFGMC. This laminate is behaving similar to the AS4/3501-6 laminate in the first test and the previous (90°/±30°/90°) laminate in which there is a clear variability among criteria for damage initiation, but all the failure criteria are very close for predicting final failure.

0° lamina, E-glass/MY750/HY917/DY063: σ_y vs σ_x failure stress envelope. A comparison of theoretical predictions to experimental for the failure stress envelope in the normal directions is shown in Figure 13(a) for GMC and Figure 13(b) for HFGMC. For the limited experimental data given, one failure criteria fits the data the best for GMC. The Tsai-Wu (Hahn) predicts the transverse compressive stress very well and follows

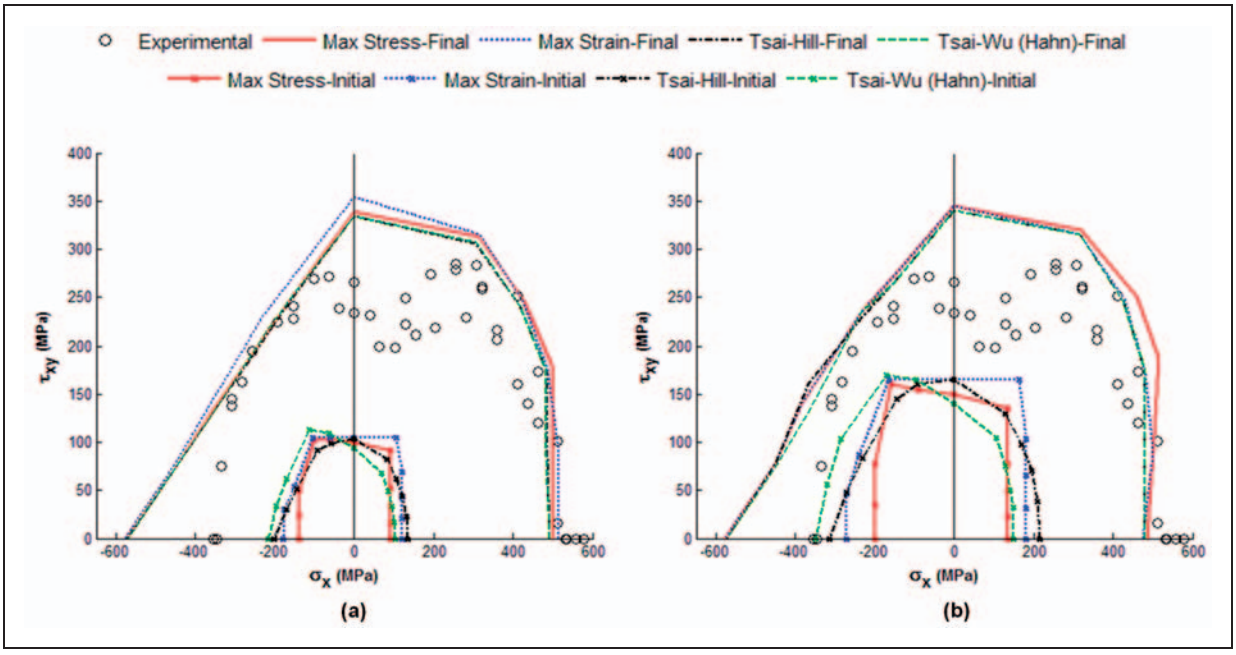

Figure 12. (90°/±30°/90°) laminate E-glass/LY556/HT907/DY063: σ_x vs τ_{xy} failure stress envelope with (a) GMC and (b) HFGMC.

Table 10. Percent error for (90°/±30°/90°) laminate E-glass/LY556/HT907/DY063 σ_x vs τ_{xy} failure stress envelope for both GMC and HFGMC

	GMC		HFGMC	
	% Error	Rank	% Error	Rank
Max stress	19.2	3	21.7	3
Max strain	21.4	4	23.2	4
Tsai-Hill	17.6	1	21.1	2
Tsai-Wu (Hahn)	17.8	2	20.4	1

GMC: generalized method of cells; HFGMC: high-fidelity generalized method of cells.

the data well within the fourth quadrant for GMC. For the HFGMC, though, Tsai-Wu (Hahn) over-predicts the transverse compressive stress but predicts the transverse tensile stress well. Table 11 confirms that the Tsai-Wu (Hahn) had the lowest error for GMC, but the over-prediction using HFGMC proved to put it last among the four theories. The disparity among the four failure theories for both GMC and HFGMC is displayed prominently for this composite system and layup. This system is very similar to the other unidirectional case, E-glass/LY556/HT907/DY063, where the final failure surfaces are very different between the various failure criteria. This shows that within a single lamina the failure criteria play a big role in dictating the shape.

(0°/90°) cross ply laminate, E-glass/MY750/HY917/DY063: stress/strain curve for σ_y:$\sigma_x = 0:1$. A comparison of theoretical predictions to experimental results for tension loading in the x-direction is shown in Figure 14(a) for GMC and Figure 14(b) for HFGMC. The experimental values are shown as open circles while the four different subcell failure criteria are shown as various denoted line types.

For both the GMC and HFGMC, the various failure criteria predictions are very similar to one another. They all over-predict the final failure by 40 MPa. For the GMC, the failure theories all follow the ε_y strain well, but the Max Strain and Tsai-Hill failure criteria follow the ε_x strain curve better than the other two failure criteria. For the HFGMC, the failure theories all follow the ε_y strain curve well with the Max Strain criterion curve now matching the other criteria curves closely. Figure 15 shows the Tsai-Hill micro plots of the two layers during loading for the GMC model where the failed subcells are circled with blue ellipses. The first failure is the matrix within the 0° layer. The second failure within the laminate is the matrix within the 90° layer. The final failure for the laminate is the fiber failure within the 90° layer, which is aligned with the loading direction in this case. The corresponding shifts in the stress–strain curve are shown in Figure 14. The failure theory that performed the best for both the GMC and HFGMC was the Tsai-Hill method, see Table 12. The large errors in the x-direction could be attributed to the small values in the strain compared to the larger values in the y-direction in the percentage error equation.

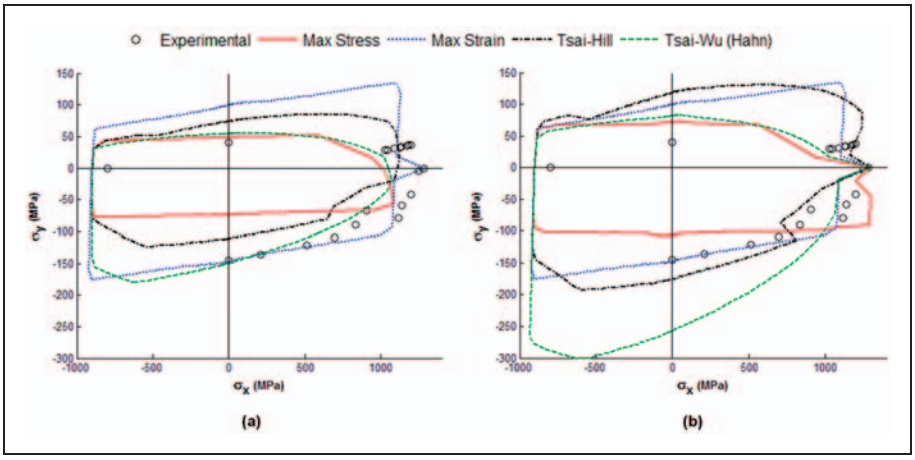

Figure 13. 0° lamina E-glass/MY750/HY917/DY063: σ_y vs σ_x failure stress envelope with (a) GMC and (b) HFGMC.

Table 11. Percent error for 0° lamina E-glass/MY750/HY917/DY063 σ_y vs σ_x failure stress envelope for both GMC and HFGMC

	GMC		HFGMC	
	% Error	Rank	% Error	Rank
Max stress	27.2	4	19.9	2
Max strain	17.4	2	17.4	1
Tsai-Hill	25.7	3	28.5	3
Tsai-Wu (Hahn)	12.3	1	30.7	4

GMC: generalized method of cells; HFGMC: high-fidelity generalized method of cells.

±55° angle ply laminate, E-glass/MY750/HY917/DY063: σ_y vs σ_x failure stress envelope. A comparison of theoretical predictions to experimental data for the failure stress envelope in the normal directions is shown in Figure 16(a) for GMC and Figure 16(b) for HFGMC. The experimental values are shown as open circles while the four different subcell failure criteria are shown as various line types. The initial failure envelope is not included because the initial envelope was only 1 to 2 MPa from the predicted final failure envelope for all failure criteria.

The simulated failure envelopes do not accurately predict the experimental data for HFGMC. Rather, the GMC captures the data set better, predicting larger failure envelopes, especially in the third quadrant. This is also apparent in the percentage errors, which were lower for GMC compared to HFGMC, Table 13. The Tsai-Wu (Hahn) criterion provided the best prediction for both GMC and HFGMC for this case. All failure theories struggled to predict accurate results in the first quadrant, with a large discrepancy along the tensile σ_y-axis. This discrepancy is explored in more detail in the next section.

±55° angle ply laminate, E-glass/MY750/HY917/DY063: stress/strain curves for σ_y:σ_x = 1:0. A comparison of theoretical predictions to experimental results for loading along the y-direction is shown in Figure 17(a) for GMC and Figure 17(b) for HFGMC. The experimental values are shown as open circles while the four different subcell failure criteria are shown as various line types.

The predictions of the various failure criteria are very similar to one another. They all under-predict the final failure significantly with very little damage progression. Neither GMC nor HFGMC correlate well with the experiments. Clearly a mechanism is not being captured by the models as the observed failure response is much more gradual and progressive than the model predictions. It is noted that the present MAC/GMC simulations are based on plate geometry for the laminate, while the experimental specimens were tubular. Bogetti et al.[36] suggest that models for this WWFE laminate must adapt to account for the fiber realignment in the tubes and also to radial expansion or contraction of the tube. This holds true for the ±55° and ±45° test specimens whose ply level strain state is dominated by shear. An improved matrix level damage progression model (beyond the step function used herein) could also potentially improve the correlation for this case. As seen in micro plots of the Tsai-Hill failure criterion, Figure 18 for GMC, the upper and lower portions of the RUC develop most of the stresses, and once the outer matrix subcells fail (those circled with blue ellipses), the damage progresses to the neighboring matrix subcells in subsequent steps, until final failure is achieved. The percent errors were not calculated since all of the failure criteria performed similarly.

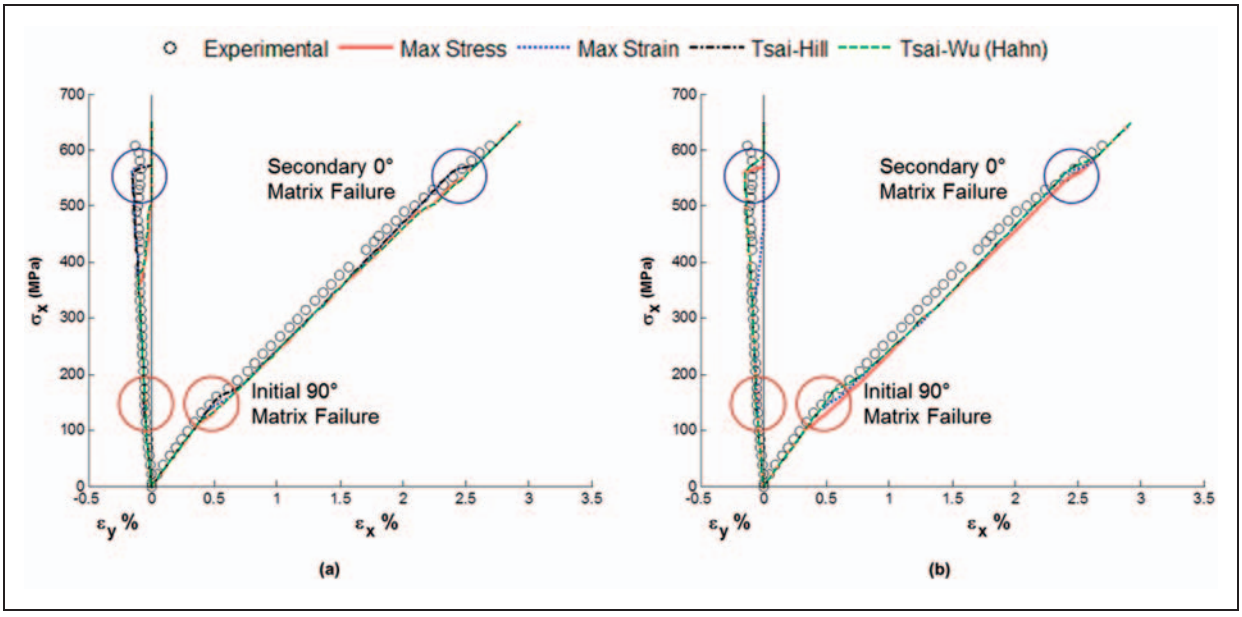

Figure 14. (0°/90°) cross ply laminate E-glass/MY750/HY917/DY063: Stress/strain curve for $\sigma_y:\sigma_x = 0{:}1$ with (a) GMC and (b) HFGMC.

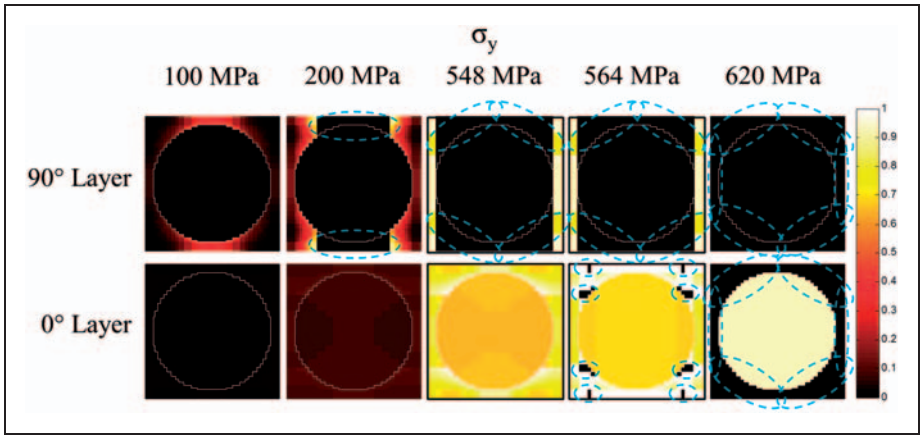

Figure 15. Tsai-Hill plots of Representative Unit Cell for (0°/90°) laminate with loading of $\sigma_y:\sigma_x = 0{:}1$ using GMC. The failed subcells are circled with blue ellipses. RUC: Representative Unit Cell.

Table 12. Percent error for (0°/90°) cross ply laminate E-glass/MY750/HY917/DY063 with loading $\sigma_y{:}\sigma_x = 0{:}1$ for both GMC and HFGMC

	GMC				HFGMC			
0/90	ε_x % error	ε_y % error	Average % error	Rank	ε_x % error	ε_y % error	Average % error	Rank
Max stress	40.9	9.8	25.4	4	26.1	10.9	18.5	3
Max strain	25.9	8.1	17.0	2	47.2	8.4	27.8	4
Tsai-Hill	25.2	7.3	16.3	1	24.3	7.4	15.9	1
Tsai-Wu (Hahn)	40.1	9.8	25.0	3	26.1	8.5	17.3	2

GMC: generalized method of cells; HFGMC: high-fidelity generalized method of cells.

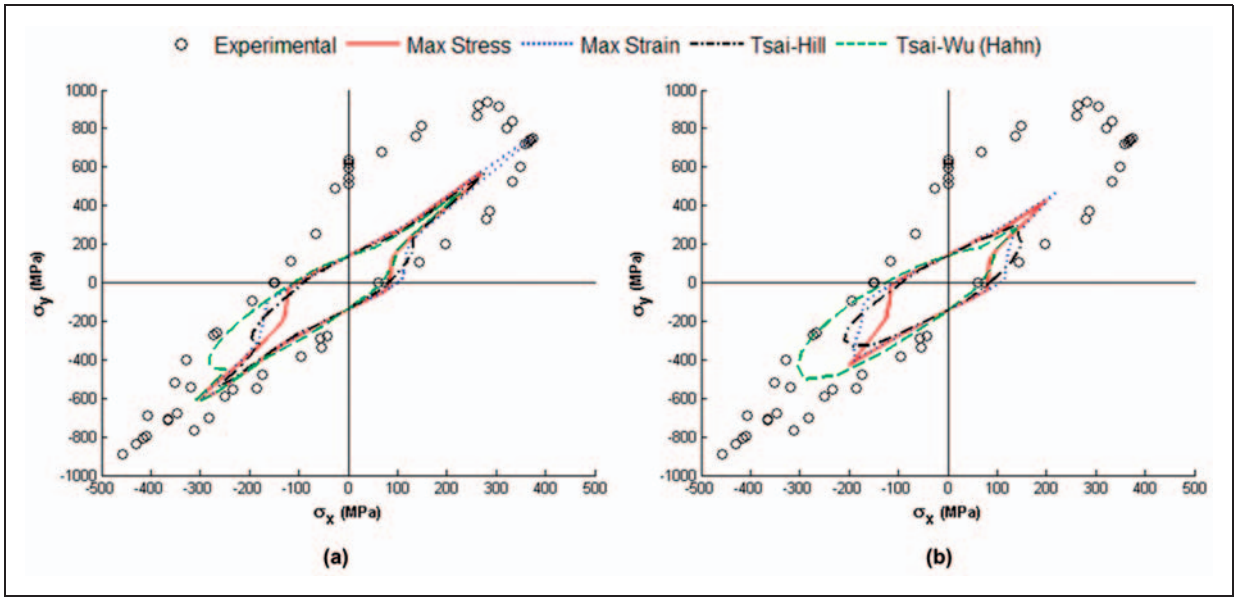

Figure 16. ±55° angle ply laminate E-glass/MY750/HY917/DY063: σ_y vs σ_x failure stress envelope with (a) GMC and (b) HFGMC.

Table 13. Percent error for ±55° angle ply laminate E-glass/MY750/HY917/DY063 σ_y vs σ_x failure stress envelope for both GMC and HFGMC

	GMC		HFGMC	
	% Error	Rank	% Error	Rank
Max stress	52.1	4	54.9	4
Max strain	47.6	2	49.4	2
Tsai-Hill	48.7	3	50.2	3
Tsai-Wu (Hahn)	44.2	1	44.3	1

GMC: generalized method of cells; HFGMC: high-fidelity generalized method of cells.

±55° angle ply laminate, E-glass/MY750/HY917/DY063: stress/strain curves for σ_y:σ_x = 2:1. A comparison of theoretical predictions to experimental results for combined tension loading is shown in Figure 19(a) for GMC and Figure 19(b) for HFGMC. The experimental values in the x-direction are shown as open circles, the experimental values in the y-direction are shown as open squares, and the four different subcell failure criteria predictions are shown as various line types.

For the GMC, there is a large deviation between the different failure theory predictions. All the theories have the same shape and capture the experimental data reasonably well. The Max Strain theory best captures the final failure, Table 14. The HFGMC, however, did not capture the failure well in this load case. It under-predicted final failure for all failure criteria, but followed the shape of the experimental curve well up until its predicted final failure.

±45° angle ply laminate, E-glass/MY750/HY917/DY063: stress/strain curve for σ_y:σ_x = 1:1. A comparison of theoretical predictions to experimental results for equal tension loading in both the x and y directions is shown in Figure 20(a) for GMC and Figure 20(b) for HFGMC. The experimental values in the x-direction are shown as open circles, the experimental values in the y-direction are shown as open squares, and the four different subcell failure criteria predictions are shown as various line types. It is noted that, for a ±45° laminate subjected to σ_y:σ_x = 1:1, there is no theoretical distinction between the ε_y and ε_x response. This should be the case for the experiments as well, but applying inner pressure to the tube specimens combined with tension produced slightly varied values for the strains.

The various failure criteria predictions are very similar to one another for both the GMC and HFGMC. All of the failure criteria follow both the ε_x and ε_y curves very well. They all captured the initial failure that changed the slope for the stress–strain plot. The models did, however, over-predict the final failure significantly, by approximately 200 MPa. The Max Stress failure theory provided the lowest percent error between the failure theories, Table 15.

±45° angle ply laminate, E-glass/MY750/HY917/DY063: stress/strain curve for σ_y:σ_x = 1:−1. A comparison of theoretical predictions to experimental results for y-directional tension and x-directional compression is shown in Figure 21(a) for GMC

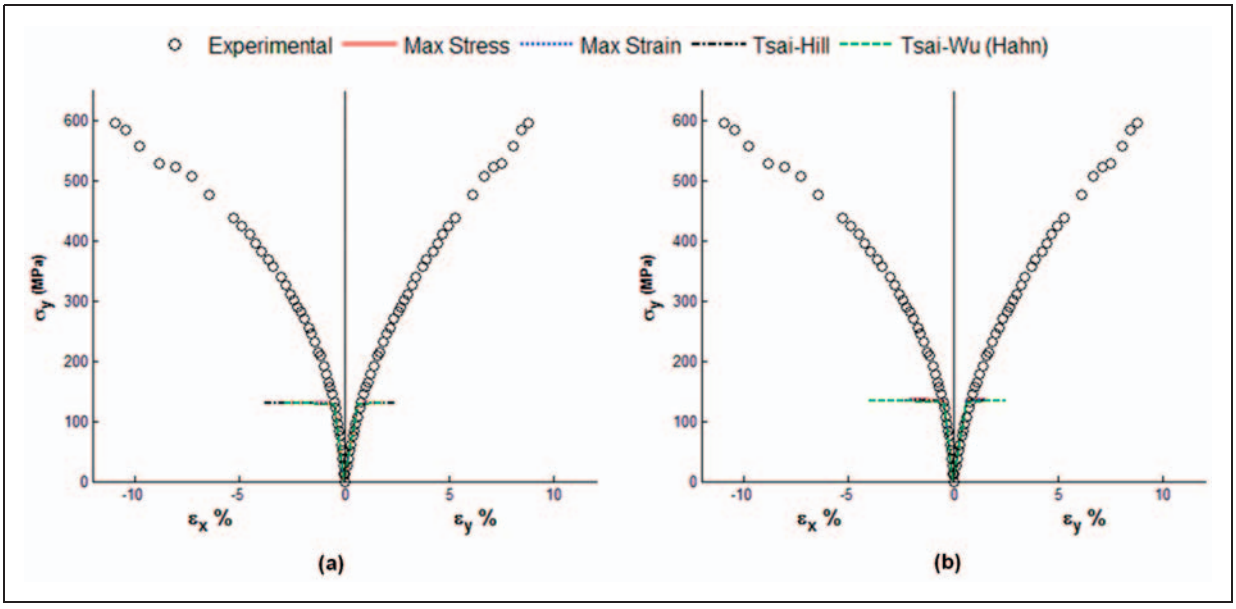

Figure 17. ±55° angle ply laminate E-glass/MY750/HY917/DY063: Stress/strain curves for $\sigma_y : \sigma_x = 1 : 0$ with (a) GMC and (b) HFGMC.

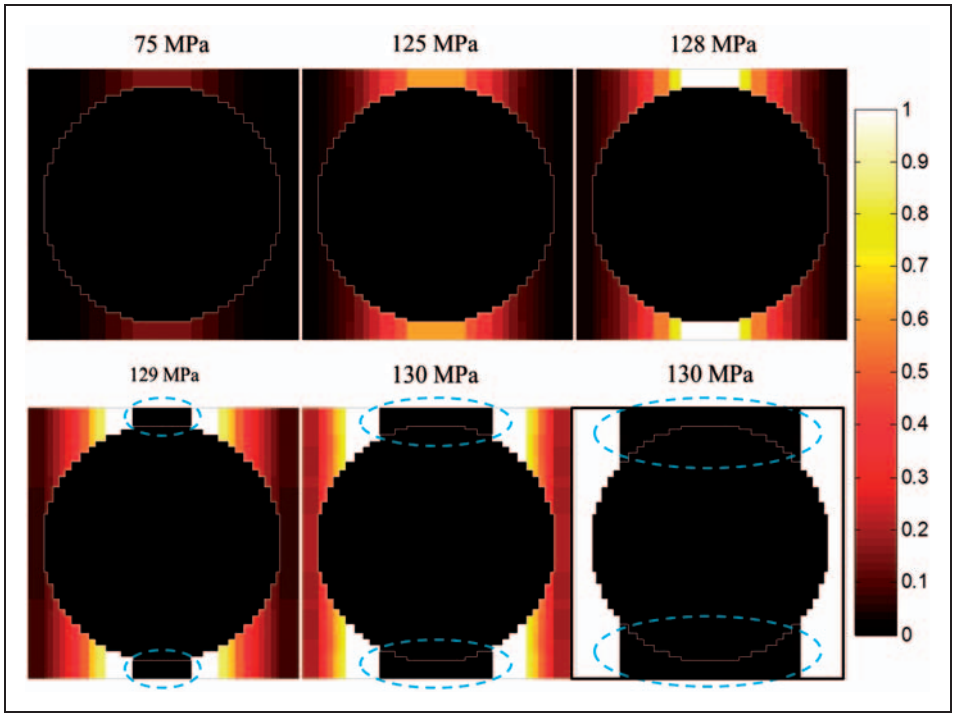

Figure 18. Tsai-Hill plots of Representative Unit Cell for ±55° laminate with loading $\sigma_y : \sigma_x = 1 : 0$ using GMC. The failed subcells are circled with blue ellipses. RUC: Representative Unit Cell.

and Figure 21(b) for HFGMC. The experimental values are shown as open circles while the four different subcell failure criteria are shown as various line types.

The various failure criteria predictions are very similar to one another for both the GMC and HFGMC. All of the failure criteria follow both the ε_x and ε_y slope very well, but they under-predict the final failure

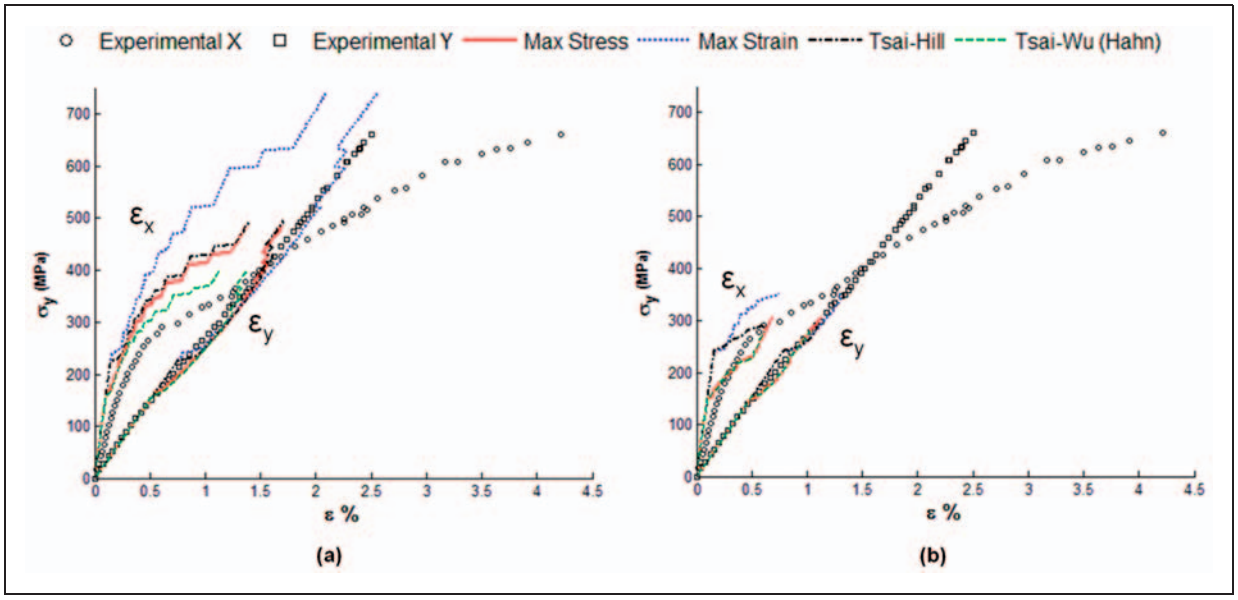

Figure 19. ±55° angle ply laminate E-glass/MY750/HY917/DY063: Stress/strain curve for $\sigma_y:\sigma_x = 2:1$ with (a) GMC and (b) HFGMC.

Table 14. Percent error for ±55° angle ply laminate E-glass/MY750/HY917/DY063 with loading $\sigma_y:\sigma_x = 2:1$ for both GMC and HFGMC

	GMC		HFGMC	
	% Error	Rank	% Error	Rank
Max stress	26.6	3	76.7	2
Max strain	12.0	1	73.4	1
Tsai-Hill	25.1	2	77.9	3
Tsai-Wu (Hahn)	39.5	4	78.8	4

GMC: generalized method of cells; HFGMC: high-fidelity generalized method of cells.

significantly, by 50 MPa. This case is similar to the ±55° angle ply laminate E-glass/MY750/HY917/DY063 under the loading ratio of $\sigma_y:\sigma_x = 1:0$, where the ply level strain state is dominated by shear. Once again, the models significantly under-predict the damage progression prior to final failure, with GMC predicting somewhat tougher laminate behavior compared to HFGMC.

Overall performance. The performance of the various failure theories was separated into two different categories: performance in stress–strain curve prediction and performance in failure surface prediction, Table 16. For the stress–strain curves, the Max Stress and Max Strain performed the best. They performed consistently toward the top for both methods of simulation, GMC and HFGMC. The Tsai-Hill failure theory and Tsai-Wu (Hahn) finished third and fourth, respectively. For the failure surfaces, it was a little more varied. For the GMC method, the Tsai-Wu (Hahn) method finished first but for HFGMC it finished third. The Tsai-Hill performed well for these cases, placing second using both GMC and HFGMC. The Max Strain criteria performed well too. It finished third using GMC and first using HFGMC. The Max Stress criteria did not perform well in predicting the failure surfaces. It placed fourth for both GMC and HFGMC analyses. These differences among the theories are caused by the multiaxial in-situ micro scale stress and strain states in each ply, which results in a predicted different initiation, and then progression, of damage for each theory.

One aspect that comes to light is that a failure theory could perform well in predicting the stress–strain curves but could be less effective in predicting the failure surfaces. The basic failure theories, Max Stress and Max Strain, kept the error lower in predicting the stress–strain curves but have a harder time calculating final failure. The failure theories that took into account the multiaxial stress states, Tsai-Hill and Tsai-Wu (Hahn), did a better job of predicting the final failures. Overall, the Max Strain failure theory was the best compromise at predicting the material behavior well in the stress–strain curves and in predicting the final failure within GMC and HFGMC.

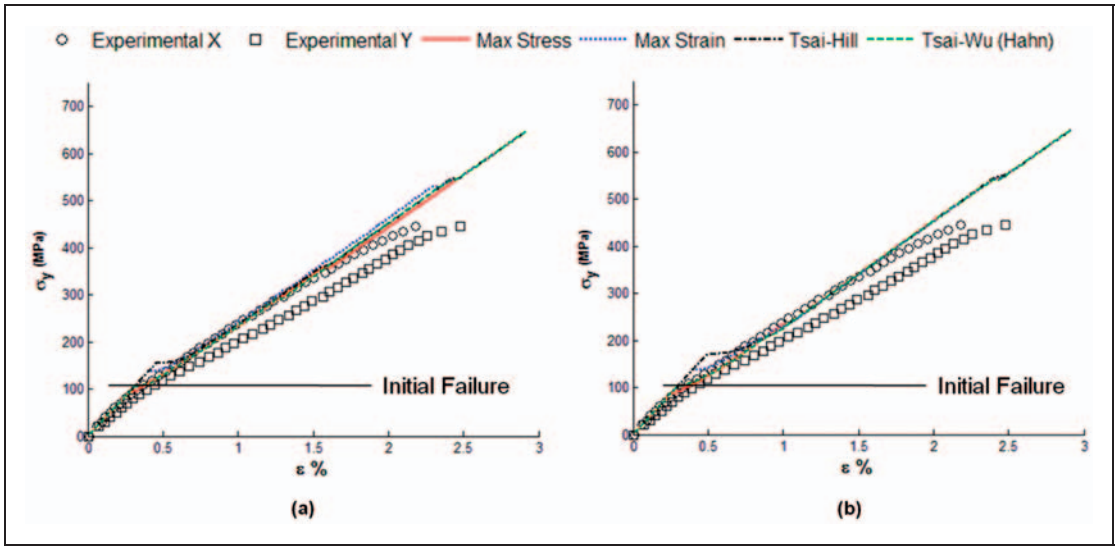

Figure 20. ±45° angle ply laminate E-glass/MY750/HY917/DY063: Stress/strain curve for $\sigma_y:\sigma_x = 1:1$ with (a) GMC and (b) HFGMC.

Table 15. Percent error for ±45° angle ply laminate E-glass/MY750/HY917/DY063 with loading σ_y:σ_x = 1:1 for both GMC and HFGMC

	GMC				HFGMC			
	ε_x % error	ε_y % error	Average % error	Rank	ε_x % error	ε_y % error	Average % error	Rank
Max Stress	3.1	16.3	9.7	1	5.1	15.6	10.4	1
Max Strain	5.4	20.1	12.8	4	5.2	18.8	12.0	3
Tsai-Hill	5.6	19.9	12.8	3	7.4	20.2	13.8	4
Tsai-Wu (Hahn)	3.7	16.6	10.2	2	5.3	15.9	10.6	2

GMC: generalized method of cells; HFGMC: high-fidelity generalized method of cells.

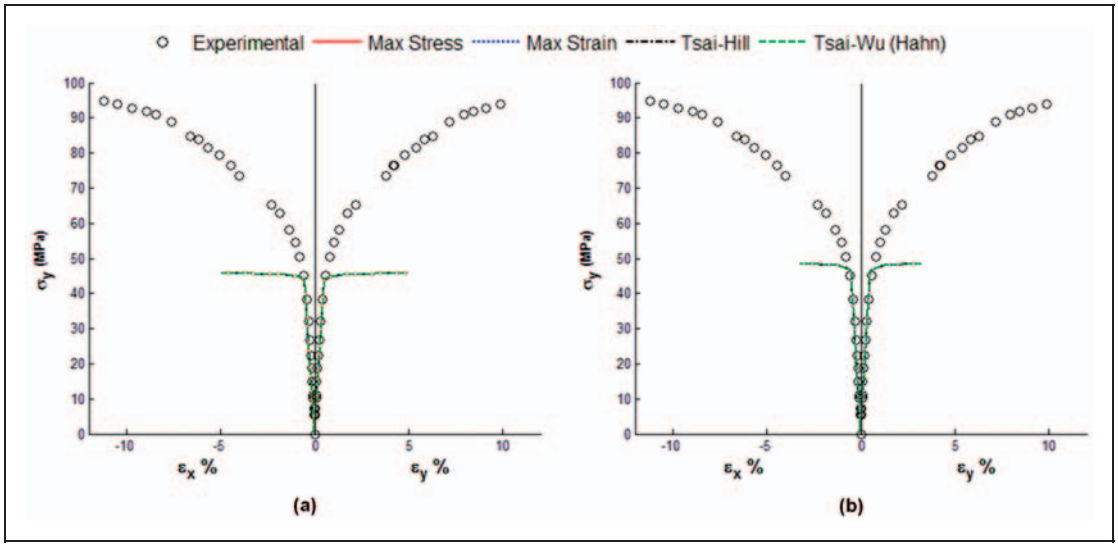

Figure 21. ±45° angle ply laminate, E-glass/MY750/HY917/DY063: Stress/strain curve for $\sigma_y:\sigma_x = 1:-1$ with (a) GMC and (b) HFGMC.

Table 16. Average ranking of percent error for various failure theories

	Stress–strain curves		Failure surface	
	GMC	HFGMC	GMC	HFGMC
Max stress	2.2	2.0	3.1	2.8
Max strain	2.0	2.4	2.5	2.2
Tsai-Hill	2.6	2.6	2.3	2.4
Tsai-Wu (Hahn)	3.2	3.0	2.1	2.6

GMC: generalized method of cells; HFGMC: high-fidelity generalized method of cells.

Conclusion

The objectives of this paper were to evaluate the basic predictive capabilities of the GMC and HFGMC micromechanics theories for the progressive failure prediction of PMC laminates and to evaluate the influence of four failure criteria applied at the fiber/matrix constituent scale. Toward this end, these two micromechanics theories (first order GMC and second order HFGMC) were used to model the ply level behavior within classical lamination theory simulations of the WWFE data. A comparison among the maximum stress, maximum strain, Tsai-Hill, and Tsai-Wu (Hahn) failure criteria was made for failure initiation, final failure, and various stress–strain curves. It must be stated that this is the first time that GMC and HFGMC have been systematically applied to predict PMC laminate failure and that no modifications were made to the fiber/matrix properties provided by the WWFE. The results are thus pure predictions from the models, without the benefit of in-situ property alterations that enable the predictions to match ply level strength data. Also, the simplest damage progression model in the form of a step function at the micro scale was used.

The results indicate that the choice of failure theory has a significant effect on the predictions, with the Maximum Strain criterion showing the best agreement with the experiments. The differences between the GMC and HFGMC micromechanics theories were small compared to those among the four failure criteria for final failure. This may be in part because the HFGMC implementation used average subcell stresses to predict failure rather than quadrature point stresses. Using average stresses negates some of the benefits of the more accurate stress concentrations provided by HFGMC and makes HFGMC act more like GMC. There is work under way to model damage at the subcell quadrature point level in HFGMC in order to capture the variation in stress and strain fields within the subcells that is missed when using subcell average quantities.

The results from this paper also show that the predictions match best with the experimental data in cases less dominated by shear at the ply and micro scales. For example, the $(0^\circ/\pm 45^\circ/90^\circ)$ AS4/3501-6 laminate predictions (Figures 4, 5, and 7) and the $(0^\circ/90^\circ)$ E-glass/MY750/HY917/DY063 laminate predictions (Figure 14) correlate well with experiment, while the $\pm 55^\circ$ E-glass/MY750/HY917/DY063 laminate predictions (Figures 16, 17, and 19) and even the shear dominated portions of the 0° lamina predictions (Figures 9 and 10) do not. There is thus a clear need for an improved damage progression model that enables a more gradual transition between failure initiation and final failure at the fiber/matrix scale, especially in cases that are dominated by local shear. The overall tendency was for the predictions to be more conservative compared to experimental failure data the more the local behavior was influenced by shear. This again points to the need for a more progressive damage model in shear that enables the dissipation of greater amounts of energy prior to final failure. Work is currently underway to address this need. It is also highly desirable to link the progressive damage to the physically meaningful fracture toughness of the material. Work is currently underway to address both of these needs.[37]

Funding

This work was supported by NASA [grant number NNX07AD70A].

References

1. Herakovich CT. *Mechanics of fibrous composites*. New York, NY: John Wiley & Sons Inc, 1998.
2. Yekani Fard M, Liu Y and Chattopadhyay A. Nonlinear flexural behavior and moment curvature response of epoxy resin using digital image correlation technique. *J Mater Sci Eng* 2011; 5: 212–219.
3. Yekani Fard M, Liu Y and Chattopadhyay A. Characterization of epoxy resin including strain rate effects using digital image correlation system. *J Aerosp Eng* 2012; 25: 308–320.
4. Yekani Fard M, Liu Y and Chattopadhyay A. Analytical solution for flexural response of epoxy resin materials. *J Aerosp Eng* 2012; Epub ahead of print. doi: 10.1061/(ASCE)AS.1943-5525.0000133.
5. Yekani Fard M, Liu Y and Chattopadhyay A. A simplified approach for flexural behavior of epoxy resin materials. *J Strain Anal Eng Des* 2012; Epub ahead of print. doi: 10.1177/0309324711430023.
6. Yekani Fard M, Chattopadhyay A and Liu Y. Multilinear stress-strain and closed-form moment curvature response of epoxy resin materials. *Int J Mech Sci* 2012; 57: 9–18.
7. Boyce MC and Arruda EM. An experimental and analytical investigation of the large strain compressive and tensile response of glassy polymers. *Polym Eng Sci* 1990; 30: 1288–1298.

8. Gilat A, Golberg RK and Roberts GD. Strain rate sensitivity of epoxy resin in tensile and shear loading. *J Aerospace Eng* 2007; 20: 75–89.
9. G'Sell C and Souahi A. Influence of cross linking on the plastic behavior of amorphous polymers at large strains. *J Eng Mater-T* 1997; 119: 223–227.
10. Hasan OA and Boyce MC. A constitutive model for the nonlinear viscoelastic viscoplastic behavior of glassy polymers. *Polym Eng Sci* 1995; 35: 331–344.
11. Liang YM and Liechti KM. On the large deformation and localization behavior of an epoxy resin under multiaxial stress state. *Int J Solids Struct* 1996; 33: 1479–1500.
12. Mulliken AD and Boyce MC. Mechanics of the rate-dependent elastic-plastic deformation of glassy polymers from low to high strain rates. *Int J Solids Struct* 2006; 43: 1331–1356.
13. Jones RM. *Mechanics of composite materials*. New York, NY: Hemisphere, 1975.
14. Bednarcyk BA and Arnold SM. *MAC/GMC 4.0 user's manual*. NASA/TM—2002-212077, 2002.
15. Hinton MJ and Soden PD. Predicting failure in composite laminates: background to the exercise. *Compos Sci Technol* 1998; 58: 1001–1010.
16. Soden PD, Hinton MJ and Kaddour AS. Lamina properties, lay-up configuration and loading conditions for a range of fibre reinforced composite laminates. *Compos Sci Technol* 1998; 58: 1011–1022.
17. Soden PD, Hinton MJ and Kaddour AS. A comparison of the predictive capabilities of current failure theoris for composite laminates. *Compos Sci Technol* 1998; 58: 1225–1254.
18. Soden PD, Hinton MJ and Kaddour AS. Biaxial test results for strength and deformation of a range of E-glass and carbon fibre reinforced composite laminates: failure exercise benchmark data. *Compos Sci Technol* 2002; 62: 1489–1514.
19. Hinton MJ, Kaddour AS and Soden PD. Evaluation of failure prediction in composite laminates: background to 'part B' of the exercise. *Compos Sci Technol* 2002; 62: 1481–1488.
20. Mayes JS and Hansen AC. Composite laminate failure analysis using multicontinuum theory. *Compos Sci Technol* 2004; 64: 379–394.
21. Huang ZM. A bridging model prediction of the ultimate strength of composite laminates subjected to biaxial loads. *Compos Sci Technol* 2004; 64: 395–448.
22. Aboudi J. Generalized effective stiffness theory for the modeling of fiber-reinforced composites. *Int J Solids Struct* 1981; 17: 1005–1018.
23. Aboudi J. *Mechanics of composite materials: A unified micromechanical approach*. Amsterdam: Elsevier, 1991.
24. Paley M and Aboudi J. Micromechanical analysis of composites by the generalized cells model. *Mech Materials* 1992; 14: 127–139.
25. Aboudi J. Micromechanical analysis of thermoinelastic multiphase short-fiber composites. *Compos Eng* 1995; 5: 839–850.
26. Pindera MJ and Bednarcyk BA. An efficient implementation of the generalized method of cells for unidirectional, multi-phased composites with complex microstructures. *Compos Pt B* 1999; 30: 87–105.
27. Bednarcyk BA and Pindera MJ. Inelastic response of a woven carbon/copper composite part II: micromechanics model. *J Compos Mater* 2000; 34: 299–331.
28. Aboudi J, Pindera MJ and Arnold SM. Linear thermoelastic higher-order theory for periodic multiphase materials. *J Applied Mech* 2001; 68: 697–707.
29. Aboudi J, Pindera MJ and Arnold SM. Higher-order theory for periodic multiphase materials with inelastic phases. *Int J Plast* 2003; 19: 805–847.
30. Aboudi J. Micromechanical analysis of composites by the method of cells – update. *Appl Mech Rev* 1996; 49: S83–S91.
31. Aboudi J. The generalized method of cells and high-fidelity generalized method of cells micromechanical models – a review. *Mech Adv Mater Struct* 2004; 11: 329–366.
32. Tsai SW. Strength theories of filamentary structures. In: Schwartz RT and Schwartz HS (eds) *Fundamental aspects of fiber reinforced plastic composites*. New York, NY: Wiley Interscience, 1968, pp.3–11.
33. Tsai SW and Wu EM. A general theory of strength for anisotropic materials. *J Compos Mater* 1971; 5: 58–80.
34. Tsai SW and Hahn HT. *Introduction to composite materials*. Lancaster, PA: Technomic Pub. Co, 1980.
35. Gibson RF. *Principles of composite material mechanics*. Boca Raton, FL: CRC Press, 2007.
36. Bogetti TA, Hoppel CPR, Harik VM, et al. Predicting the nonlinear response and failure of composite laminates: correlation with experimental results. *Compos Sci Technol* 2004; 64: 477–485.
37. Pineda EJ, Bednarcyk BA, Waas AM, et al. Progressive failure of a unidirectional fiber-reinforced composite using the method of cells: discretization objective computational results. In: *Proceedings of the 53rd AIAA/ASME/ASCE/AHS/ASC structures, structural dynamics and materials conference*, Honolulu, HI, April, 2012, AIAA, pp.2012–1539.